Pulse Compression in TTF Injector II

J.B. Rosenzweig
Department of Physics
University of California, Los Angeles

March 6, 1995

I. Analytical Approach

While the description of the longitudinal dynamics of a beam in an rf photo-injector is in general quite complicated, the problem is straightforward after some simplifying assumptions. It is in fact an excellent assumption, that after acceleration to moderately high energy, where the longitudinal space charge forces are negligible compared to the applied rf forces, that the longitudinal phase space structure is well approximated by that of a beam which has passed through the accelerating cavities at the speed of light. Under this assumption, each electron has a final energy given by

$$E(\phi) \cong E_m \cos(\phi),$$

where ϕ is the accumulated rf phase of the electron, which is taken to be the injection phase plus a constant (the same for all electrons) dependent on the gun dynamics and linac phasing, and E_m is the maximum possible electron energy obtained at the optimum phase. We have implicitly ignored the rf phase compression and the phase expansion due to space charge at low energy. Both of these effects are mild, however, and tend to cancel each other in practice. The expansion of the pulse due to space charge is a second order effect - the first order effect is a front-to-back energy slew which is approximately linear, and therefore has the effect of changing the effective injection phase of the bunch.

Using these preliminary considerations, it is straightforward to formulate an rms treatment of the longitudinal phase space, in direct analogy with the familiar transverse Twiss parameter formalism. We state the results of this development, leaving the details of the derivation to the interested reader.

The longitudinal emittance is given by

$$\varepsilon_\phi \equiv \sqrt{\left\langle \phi^2 \right\rangle \left\langle \left(\frac{\Delta p}{p}\right)^2 \right\rangle - \left\langle \phi \frac{\Delta p}{p} \right\rangle^2} \cong \tfrac{1}{2} \sigma_\phi^3 \cos(\phi_0),$$

where $\sigma_\phi = \sqrt{\langle \phi^2 \rangle}$, and the longitudinal phase space variables have been chosen as the rf phase and the relative momentum spread (which is taken to be identical to the relative energy spread for these ultra-relativistic beams). The beta-function is therefore

$$\beta_\phi \equiv \frac{\langle \phi^2 \rangle}{\varepsilon_\phi} \cong \frac{2\cos(\phi_0)}{\sigma_\phi},$$

and the correlation function is

$$\alpha_\phi \equiv -\frac{\langle \phi \frac{\Delta p}{p} \rangle}{\varepsilon_\phi} \cong \frac{1}{\sigma_\phi}\tan(\phi_0).$$

The final longitudinal rms Twiss parameter is related to the momentum spread,

$$\gamma_\phi \equiv \frac{\left\langle \left(\frac{\Delta p}{p}\right)^2 \right\rangle}{\varepsilon_\phi} = \frac{1+\alpha_\phi^2}{\beta_\phi}$$

It is straightforward to show that the maximum compression factor one can obtain through a chicane transformation (a "drift" in longitudinal phase space), is

$$r_c = \sqrt{\alpha_\phi^2 + 1}.$$

This compression ratio is obtained for a particular value of

$$R_{56} \equiv \frac{\partial \phi}{\partial\left(\Delta p/p\right)} = \frac{\alpha_\phi \beta_\phi}{r_c^2} = \frac{\beta_\phi}{\alpha_\phi - \alpha_\phi^{-1}}$$

which is of course dependent on the chicane design. A particular standard chicane design is discussed in some detail below.

The unitless phase space variables can be converted to physical units by multiplying the coordinates (ϕ, β and R_{56}) by $\lambda_{rf}/2\pi$, and the momenta ($\Delta p/p$) by p. The emittance is naturally then converted to physical units by multiplying by $\lambda_{rf} p/2\pi$.

II. A Compressor Beam Line

The layout shown in Figure 1 shows a symmetric four bend compressor chicane which is dispersion free to all orders in the absence of space charge. In this chicane all of the magnets have equal lengths and radii of curvature. The displacements between the magnets where the trajectories are at an angle with respect to the nominal beam line are equal. The gap between the second and third bends, which is may be chosen with some freedom in length, subject to alignment tolerance and space charge concerns, is needed for placement of a momentum collimator. The introduction of space charge gives rise to effects such as dispersion mismatch, which will be discussed further below. Before examining these more subtle effects, however, it is instructive to examine the linear optics of such a compressor.

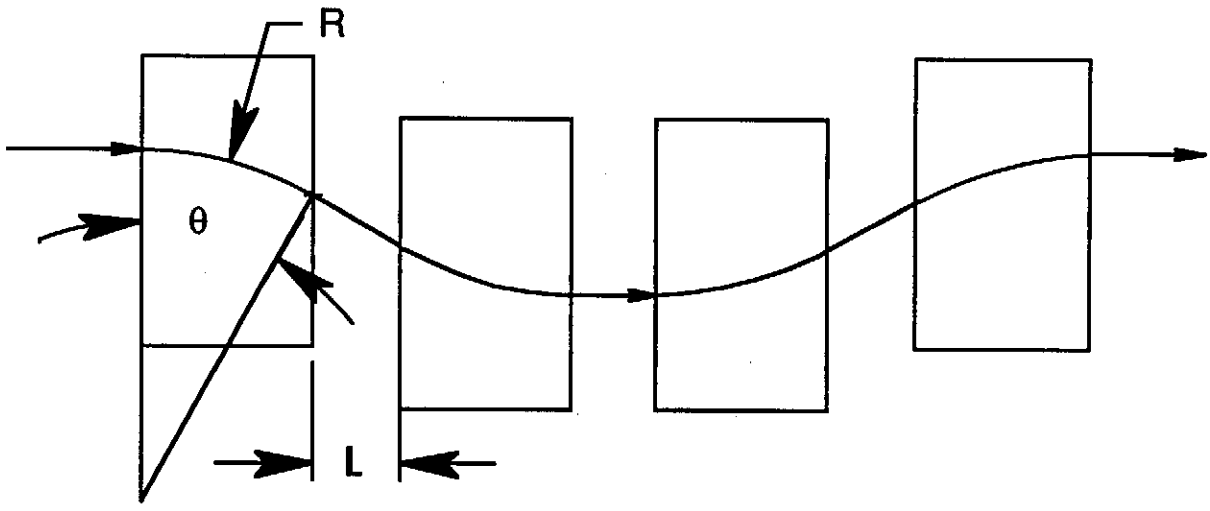

Figure 1. A symmetric four bend chicane, which gives compression with a negative R_{56}.

It can be seen by inspection of Fig. 4 that the dispersion function is symmetric about the midplane of the chicane. The maximum dispersion at the midplane, where momentum spread measurement as well as correction with collimation can be optimally performed, is

$$\eta_{x,\max} = 2R\left[1-\cos(\theta)\right] + L\frac{\sin(\theta)}{\cos^2(\theta)}.$$

From the horizontal dispersion, we obtain the linear transport matrix element, the "time dispersion",

$$R_{56} \equiv \int \left(\frac{1}{\gamma^2} - \frac{\eta_x(s)}{R} \right) ds = \frac{1}{\gamma^2} \left(L\left(\frac{2}{\cos(\theta)} + 1 \right) + 4R\theta \right) + 2R[\theta - \sin(\theta)] + L\left(\frac{\theta \sin(\theta)}{\cos^3(\theta)} \right).$$

Assuming the willingness to allow small changes to the vacuum beam pipe system, it can be seen that this is a very flexible chicane in terms of the time dispersion. It should be noted that there is essentially no horizontal focusing in this chicane, while there is quite strong vertical focusing due to the dipole edge angles. In order to keep the vertical focusing from being too strong, this implies use of small bend and edge angles. At the same time, for relatively modest values of α_ϕ (and thus the off-crest phase of the linac), the time dispersion must be large. This then dictates the radii of curvature or drift lengths, or combination of both, that one must use.

One further note about this choice of chicane, and that is that the R_{56} is positive, meaning that high energy particles are pushed forwards towards the leading edge of the bunch. For a system with space charge this has two implications. The first is that this compressor demands a positive value for α_ϕ, which is the opposite of the slope in longitudinal phase space naturally produced by space charge, and thus the linac must be rephased to put the bunch further forward of the peak acceleration crest to compensate for this effect (the gun is not in general rephased, because of transverse emittance considerations). The second implication of the positive R_{56} is that the longitudinal space charge is that it works in opposition to the compressing motion within the chicane itself. This dynamic opposition provides a slight stabilizing effect on phase and charge errors. Conversely, a negative R_{56} implies a compressor running in a "negative mass" instability regime characteristic of circular accelerators run below transition, in which fluctuations in charge will be magnified in the compressor.

It has also been noted by Carlsten[1] that this type of compressor has a relatively long path length, which can add to the emittance growth problems encountered. As an alternative, he has suggested circular (alpha magnet-like) compressors, which have a negative R_{56}. We do not consider this type of compressor here, as it increases the complexity of the beamline layout in the TTF hall considerably.

III. Envelope Calculations With Space Charge

The program TRACE 3D[2] models all of linear transport as well some higher order effects. Of particular to this discussion, it includes a three-dimensional space charge model based on Kapchinskii-Vladimirski theory, as well as the notion of rms equivalent uniform beam. TRACE 3D calculations will therefore yield several useful results concerning the problem of high intensity beam compression: (1) the effective dephasing of the bunch due to the linear component of the longitudinal space charge forces during transport and acceleration, and (2) the degree of horizontal emittance growth due to dispersion mismatch caused by the transverse space charge forces. This analysis serves both as a precursor to optimize the design before more detailed simulations, and to give a first estimate on the effects of fluctuations on the compressor performance.

The transport is followed from approximately the end of the second gun solenoid[3] using PARMELA output, at both the end of the focusing solenoid (after the gun) and at the linac exit, to guide the input choices. The graphical output of a TRACE 3D run is included in Figure 2 for a reference illustration. After a meter of drift, the beam is injected into a 20 MV/m average accelerating gradient TESLA standing wave superconducting cavity. The accelerating gradient used is relatively high, as one hopes to have as high an energy beam at compression as possible. Following the linac, a quadrupole triplet is used to prepare the beam asymmetrically for transport through the chicane. The beam is actually defocused in the vertical dimension in order to counteract the strong vertical focusing and keep the space charge forces smaller in the chicane by minimizing the bunch density. The horizontal beam size is of course dominated by momentum spread in the compressor, and the beam is focused horizontally to come to a betatron waist near the end of the chicane, a condition which mitigates the dispersion mismatch at the compressor exit due to space charge by minimizing the beam size and maximizing the betatron angular divergence at that point.

The properties of the chicane and the nominal 8 nC TTF beam used as input are summarized in Table 1. The results of the TRACE 3D calculations regarding the performance of this compressor as a function of linac phase - bunch length, energy spread, and emittance growth due to dispersion mismatch - are summarized in Fig. 3. The compressed beam shows a moderate emittance growth, and compression of over a factor of five in bunch length.

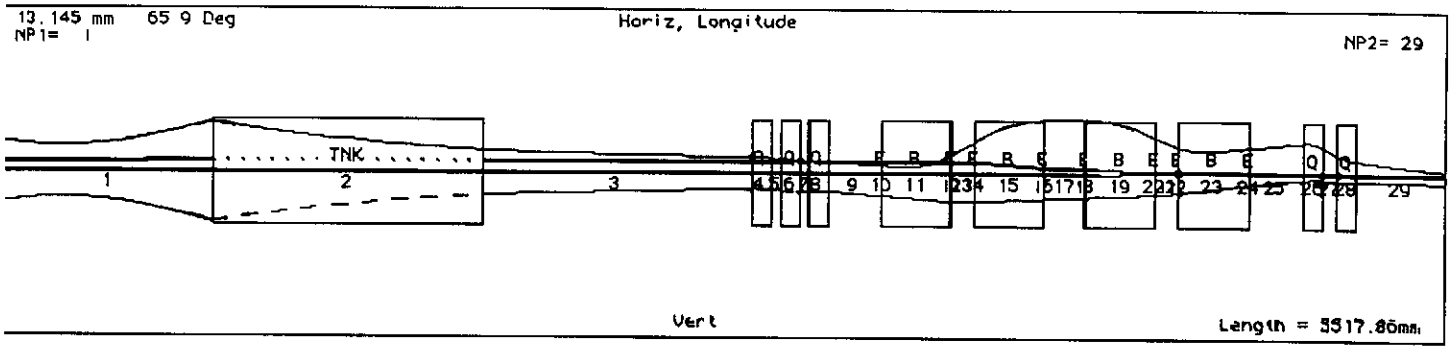

Figure 2. TRACE 3-D simulation graphical output for TTF photoinjector beam from exit of gun focusing system through TESLA linac section with average accelerating gradient of 15 MV/m, transport and compression chicane.

Bend angle θ	22.5°
Bend radius R	70 cm
Drift $L/\cos(\theta)$	8.5 cm
Time dispersion R_{56}	0.100
Maximum compression	5.6
Input beam energy	3.5 MeV
Average optimum linac gradient	17 MV/m
Initial normalized rms emittance ε_x	14 mm-mrad
Bunch charge	8.3 nC
Initial rms bunch length	4.1 mm
Final rms longitudinal emittance ε_z	450 mm-keV

Table 1: Parameters of input beam and chicane for high bunch charge compressor.

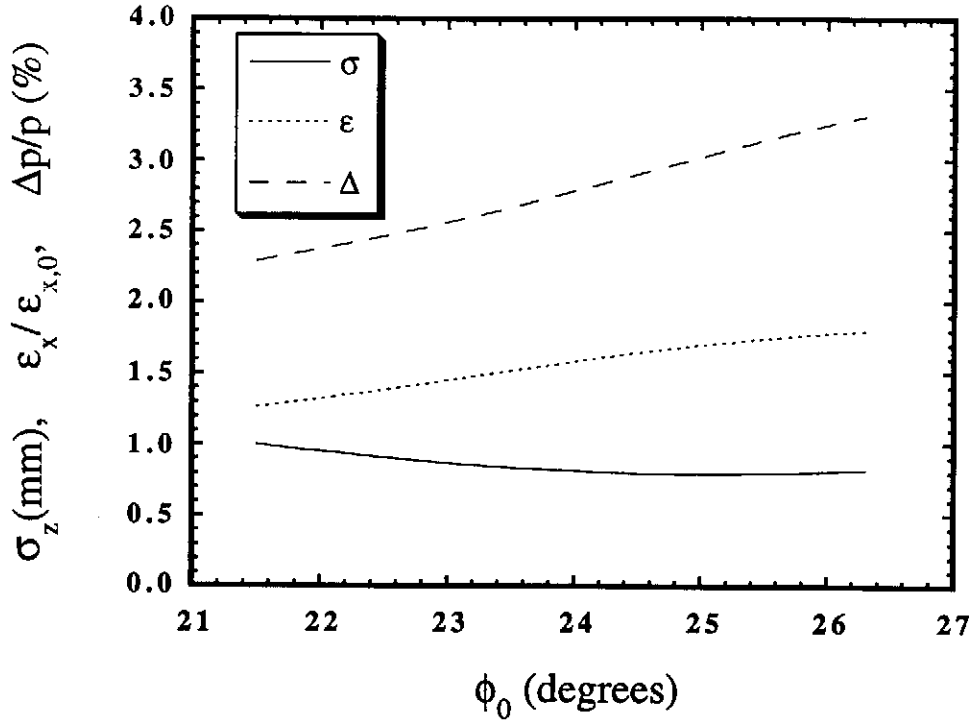

Figure 3: Rms bunch length, emittance, and relative momentum spread, as a function of linac phase, from TRACE 3D calculation, with compressor and input beam of Table 1.

IV. Scaling in compression: the low charge case.

Previous investigations of the behavior of an emittance compensated rf photoinjector operating in the space-charge emittance dominated regime have shown that the compensation performance of a photoinjector is essentially unchanged by scaling the beam dimensions[4] all as

$$\sigma_i \propto Q^{1/3}.$$

Under these conditions, the transverse emittances scale as

$$\varepsilon_{x,y} \propto Q^{2/3},$$

and the transverse beta-functions are unchanged.

The longitudinal emittance likewise scales as

$$\varepsilon_\phi \propto \sigma_z^3 \propto Q,$$

while the beta-function scales as

$$\beta_\phi \propto \sigma_z^{-1} \propto Q^{-1/3},$$

and the correlation function also scales as

$$\alpha_\phi \propto \sigma_z^{-1} \propto Q^{-1/3}.$$

This implies that, in analogy to the rf photoinjector and its focusing optics, the same compressor, using the identical chicane and rf phase, will optimally compress this beam, but by a larger factor. This analogy holds strictly, however, only in the absence of space charge. For large correlation functions, the compression factor scales approximately as

$$r_c \approx \alpha_\phi \propto Q^{-1/3}.$$

Thus the final beam length, after compression, therefore scales as

$$\sigma_z \propto Q^{2/3}.$$

For the SASE FEL operation presently under study at DESY[5], the bunch charge is taken to be 1 nC, with an emittance, following this scaling, of 3.5 mm-mrad, or 4 times smaller than the 8 nC case. The initial rms pulse length is 2.06 mm for this charge. The rest of the scaling laws have been followed in generating TRACE 3-D simulations, with the results shown in Fig. 4.

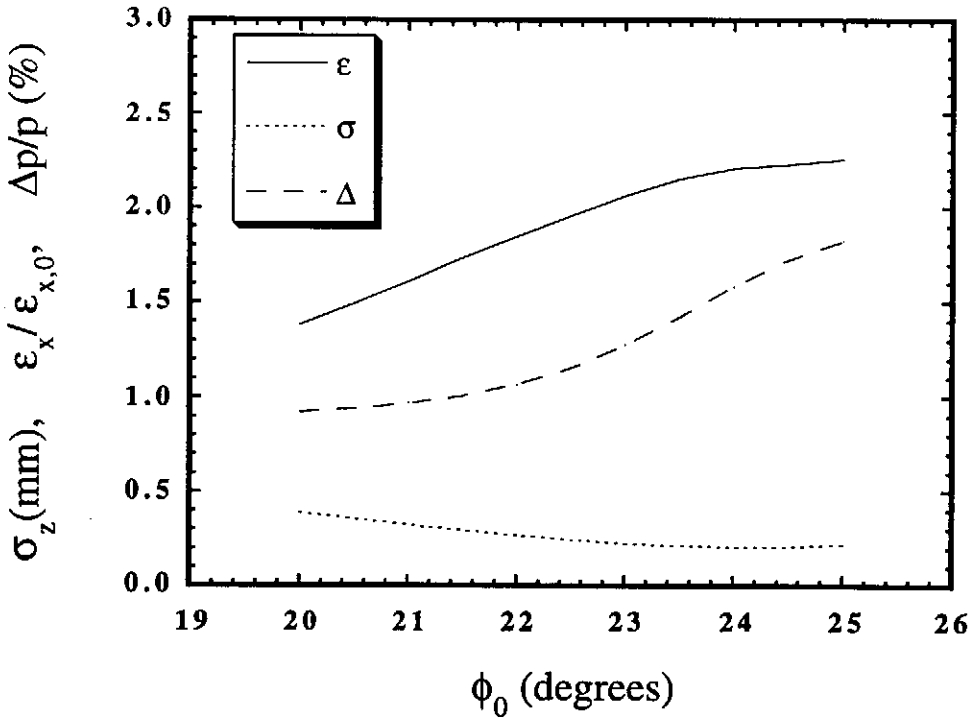

Figure 4: Rms bunch length, emittance, and relative momentum spread, as a function of linac phase, from TRACE 3D calculation, with compressor and input beam of Table 1, beam parameters scaled to 1 nC.

It can be seen that the relative growth in the energy spread is larger in this case, as the longitudinal space charge becomes more significant because the nominal compression factor is larger (it is now 11.2 in the absence of space charge - with space charge it is approximately 10, as can be seen in Fig. 3). An additional effect of this enhanced compression is that the relative emittance growth due to dispersion mismatch is noticeably larger. If one operates the linac at a smaller phase offset, the compression factor is smaller and the associated emittance growth is mitigated. Under these conditions the beam is not optimally matched to the compressor, that is it does not come to a longitudinal waist, and the compressed beam will be more sensitive to laser injection phase fluctuations.

V. PARMELA simulations: details of the beam distribution

The accurate simulation of the compression process with a code such as PARMELA is much more difficult than the simulation of the axisymmetric portions of the photoinjector up to the end of the linac. This is because the beam's space charge

forces must be calculated in three dimensions instead of two. For PARMELA, this means abandoning the r-z mesh calculation, which has a CPU time dependence linear in the number of simulation particles N, in favor of a point-by-point calculation, which has a computation time quadratic in N. In addition, our version of PARMELA does not at present use retarded potentials to calculated the fields, an omission which may be important for beams which are bending, and therefore have strong differential accelerations and velocities. A final caveat is to note that for a reasonable calculation time, we must limit $N<2000$, at which point the coarseness of the distribution gives rise to computational noise, leading to false emittance growth.

With all of these issues in mind, it is still quite useful to show the results of PARMELA simulation, as the details of the phase and configuration space distributions can be examined. In particular, one can directly observe the effects of collimating cuts on the phase space distributions. It is implicit in our design philosophy for the TTF photoinjector that collimation of the beam to 80 percent of the launched charge be performed to clean up both the longitudinal and the transverse emittances. This collimation is naturally performed at the high dispersion point of the compressor. Here the collimated beam particles consist mainly of those at the front and back of the beam pulse, which have both the highest relative momentum deviations and large betatron excursions, since they have "crossed over", and have much different phase space trajectories than those in the beam core, which have mainly laminar trajectories.

The performance of the high charge beam in the compressor was examined without much (time-consuming) attempt at optimization. The beam parameters we quote here are full rms, as opposed to the more sophisticated phase space diagnostics used in describing the photoinjector beams. The gradient assumed in the superconducting linac section is limited by the allowable rf focusing kick, which can cause cross-over in the transverse phase space, thus degrading the initial normalized emittance. The momentum collimating cut, placed in the middle of the compressor, produced a reduction in the rms momentum spread of approximately twenty percent. The beam parameters in the simulation are given in Table 2 - there are slight insignificant disagreements between Tables 1 and 2, due to the presence of the "guard charge" which is collimated in the PARMELA simulations. Note that the compression is larger than one might first expect, over a factor of 6, due to the collimation of the momentum distribution and thus the longitudinal emittance. This again illustrates that a compressor designed for a particular ε_ϕ will compress the bunch length by a factor proportional to $\varepsilon_\phi^{1/3}$, as was seen in the discussion of the low charge case.

Beam final energy	20.2 MeV
Initial charge	10 nC
Rms momentum spread (precompress)	2.25 %
Rms normalized emittance (precompress)	13.8 mm-mrad
Rms bunch length (precompress)	4.1 mm
Initial longitudinal emittance	525 mm-keV
Linac phase	22 degrees
Final charge	8 nC
Final rms momentum spread	2.6 %
Final rms normalized emittances	$\varepsilon_{y,x} = 13.4, 30.2$ mm-mrad
Final rms bunch length	0.98 mm
Final longitudinal emittance	355 mm-keV

Table 2. Beam parameters from PARMELA simulation with point-by-point space charge calculation. Initial parameters are directly before the first quadrupole.

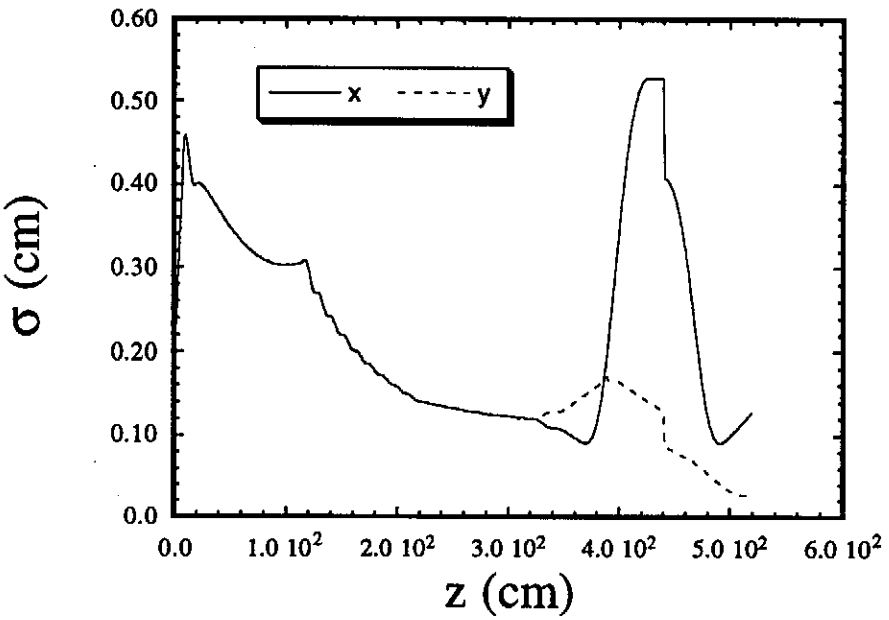

Figure 5. Beam envelopes from cathode through compressor, 8 nC case. Note that the beam envelope is similar to the TRACE 3D output, but with discontinuities associated with the collimating cut taken in the middle of the compressor.

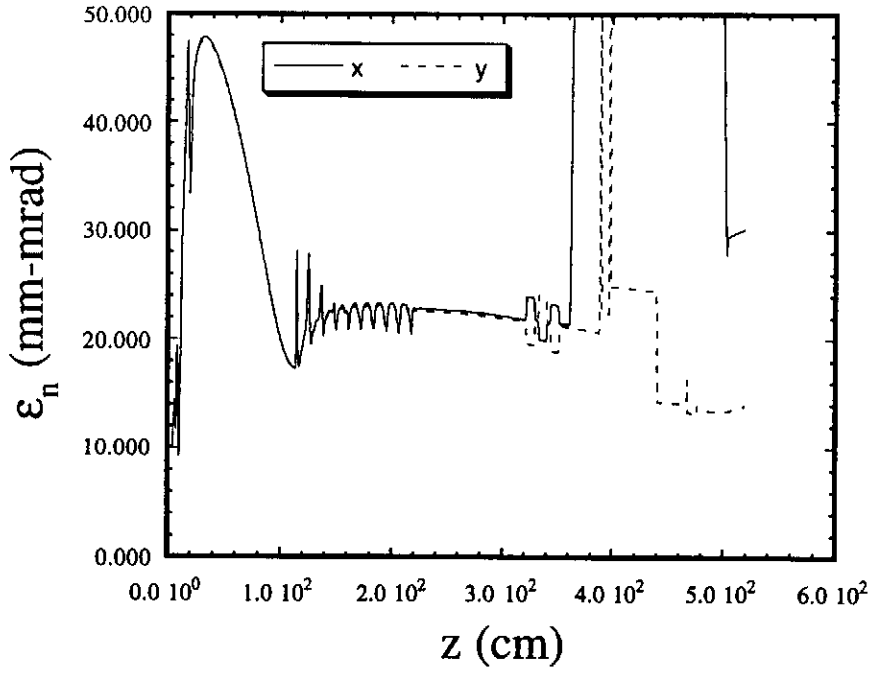

Figure 6. Emittance evolution in 8 nC case. Note effect of the collimating cut on the vertical emittance.

It is instructive to view the distributions generated by simulation. Figure 7 shows the longitudinal phase space distribution, with configuration space compression as well as the associated momentum spread heating due to enhanced longitudinal space charge forces. It can be seen that the long tail due to higher energy particles is difficult to suppress without removing too many beam particles with this phase of the linac, which is already quite large. This is a function of the excessive curvature of the phase space distribution, a point which will be discussed further below. The associated current profile, shown in Figure 8, clearly displays a sharp rising edge and long tail. From the point of view of TTF experiments, the most relevant quantity may be the spectral content, however, not the microscopic details of the current profile. The FFT of this profile is displayed in Figure 9, along with the equivalent spectrum of a gaussian current profile with the identical rms width. It is not yet clear what the impact of the non-gaussian current profile on HOM analysis at TTF and TESLA; this is an area that demands future study.

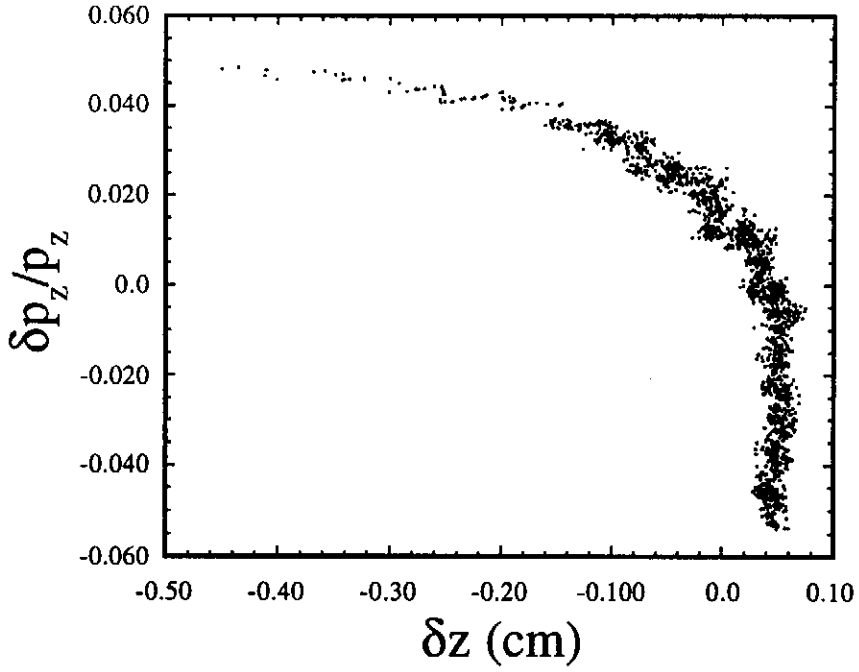

Figure 7. The longitudinal phase space after compression and collimation, 8 nC case.

The equivalent change in effective linac phase (on the longitudinal phase space presented to the compressor entrance) with space charge variations was determined from PARMELA to be approximately 0.09 deg/nC. This is negligibly small, in the sense that even large variations (40%) in the beam charge due to laser fluctuations will be have less effect on the longitudinal compression than the expected 0.4 degree rms laser injection phase jitter. Space charge within the compressor, while diminishing the fluctuations in beam length slightly, does so at the expense of magnifying the energy spread (the longitudinal emittance actually decreases slightly because of collimation). The increase in the energy spread is at first glance disturbing, as the temptation is to conclude that the longitudinal space charge forces are large after the compressor. This is not quite true - the maximum longitudinal space charge force on the beam edges at the end of the compressor is approximately 200 keV/m. Much of the changes in the energy distribution come in the compressor due to the work done on the electrons by the transverse space charge electric field as the derivative of the dispersion function becomes large. This effect can quantified as follows,

$$\left.\frac{dE}{dz}\right|_{\delta p/p} \approx -eE_{x,sc}\eta_x' \frac{\delta p}{p}.$$

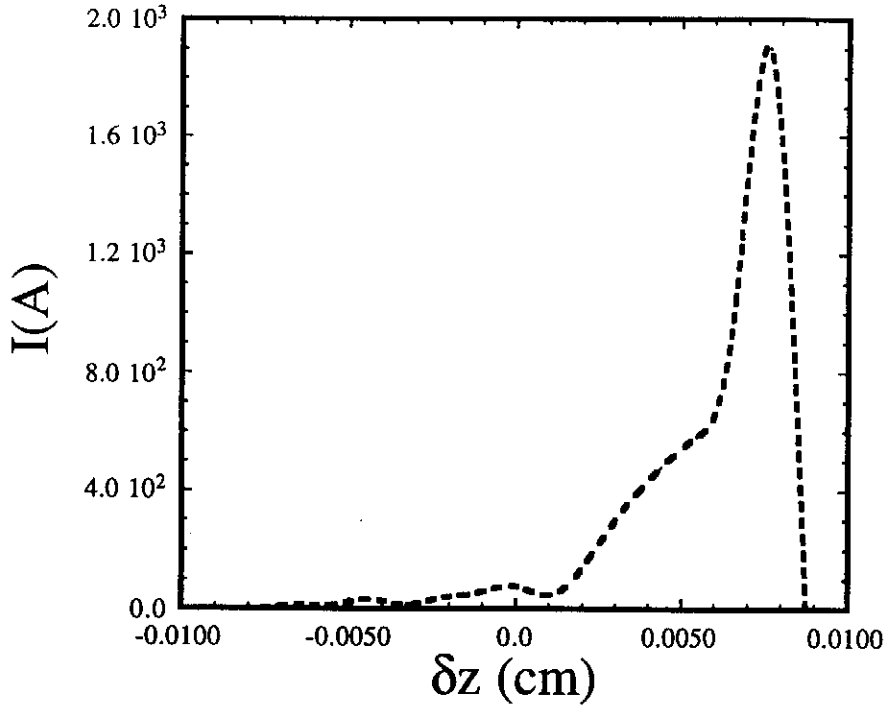

Figure 8. The current profile associated with the phase space distribution in Fig. 7.

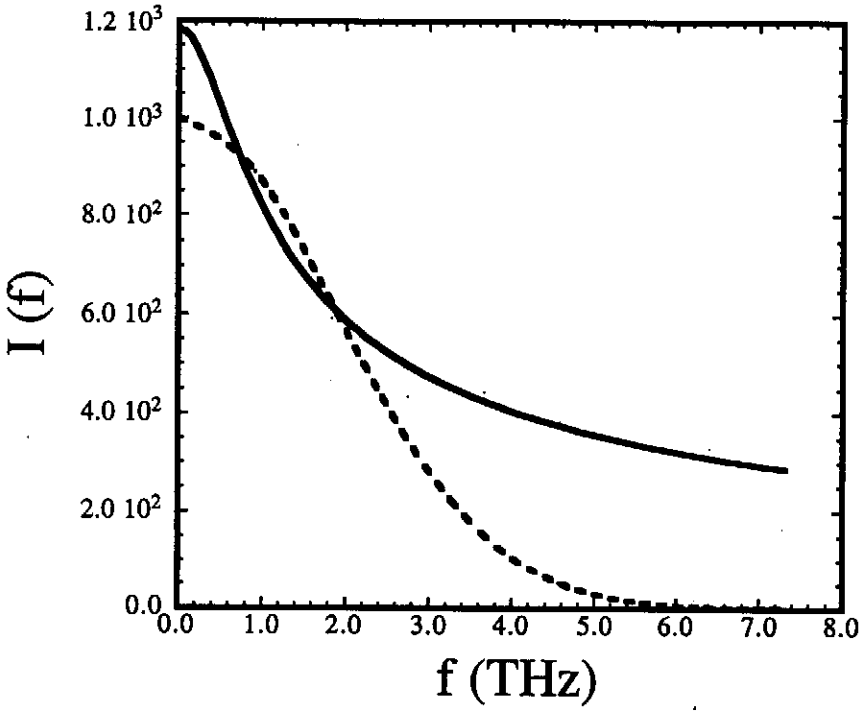

Figure 9. The FFT spectrum of the current profile in Fig. 8, with the spectrum of a gaussian with 1 mm rms length shown (dashed line) for comparison.

This effect causes a large energy change in the final magnet, where the beam is nearly fully compressed, making the transverse space charge electric field large, and the derivative in the dispersion relation is also large. The sign of the force changes from one side of the beam to the other, as does the sign of $\delta p/p$, and so this energy variation has the same sign regardless of $\delta p/p$ - it is decelerating in the final dipole, as the electrons give up kinetic energy to create field energy. This can be seen by the long low energy tail developing in Fig. 7. It should be noted that the inverse of this effect, in which the momentum coupling to the betatron motion through space charge forces, is the source of the dispersion mismatch which produces horizontal emittance growth.

Space charge also obviously plays a prominent role in the transverse dynamics. Figure 10 shows the horizontal phase space distribution at the exit of the triplet after the compressor. The nearly a factor of 2 increase in the emittance due to coupling with the longitudinal phase space through the dispersion mismatch is apparent in this picture.

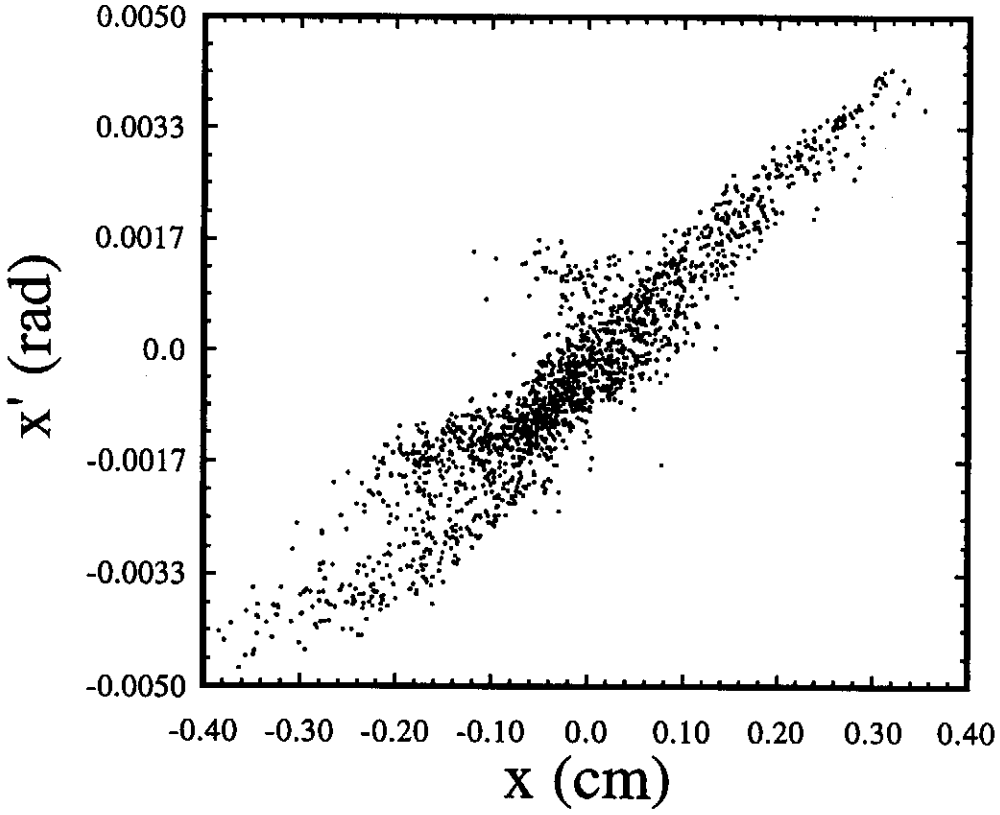

Figure 10. Transverse phase space distribution after compression and collimation, 8 nC case.

The dispersion mismatch is also noticeable in the configuration space (x-z) distribution shown in Figure 11. The "tilt" to the distribution indicates residual correlations between the longitudinal and transverse phase spaces. The tilt is more distinct in the high current part of the beam, where the space charge forces are more intense.

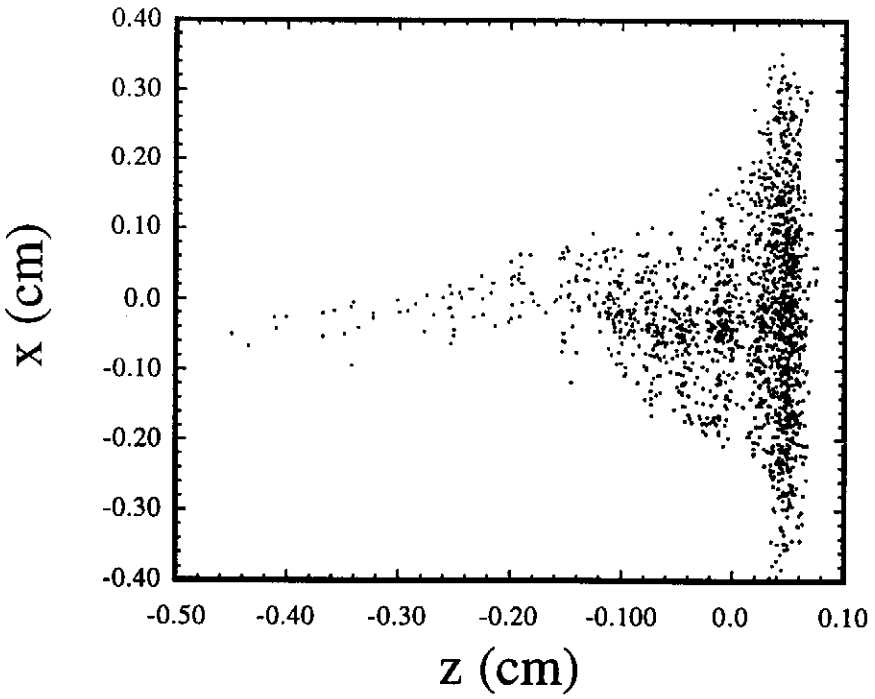

Figure 11. The configuration space distribution after compression and collimation. Note the slight tilt in the distribution due to residual dispersion.

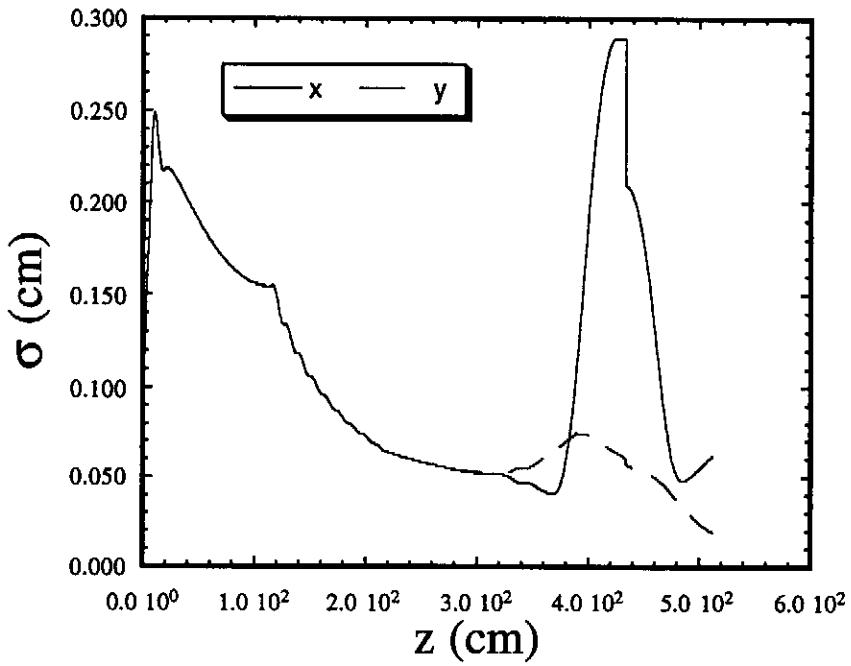

Figure 12. Rms beam envelopes in rf photoinjector, linac and compressor, 1 nC case.

The 1 nC charge case displays similar behavior in the PARMELA simulations, as can be seen in Figures 12 and 13. All of the input parameters are scaled from the 8 nC case according to the prescription given above. It should be noted that the final emittances are $\varepsilon_{y,x} = 4.6, 6.3$ mm-mrad, where the original 80% emittance before compression was 4 mm-mrad. While these are good emittances for a beam with a peak current of over 500 A, they do not meet the demands for the short wavelength FEL at DESY.

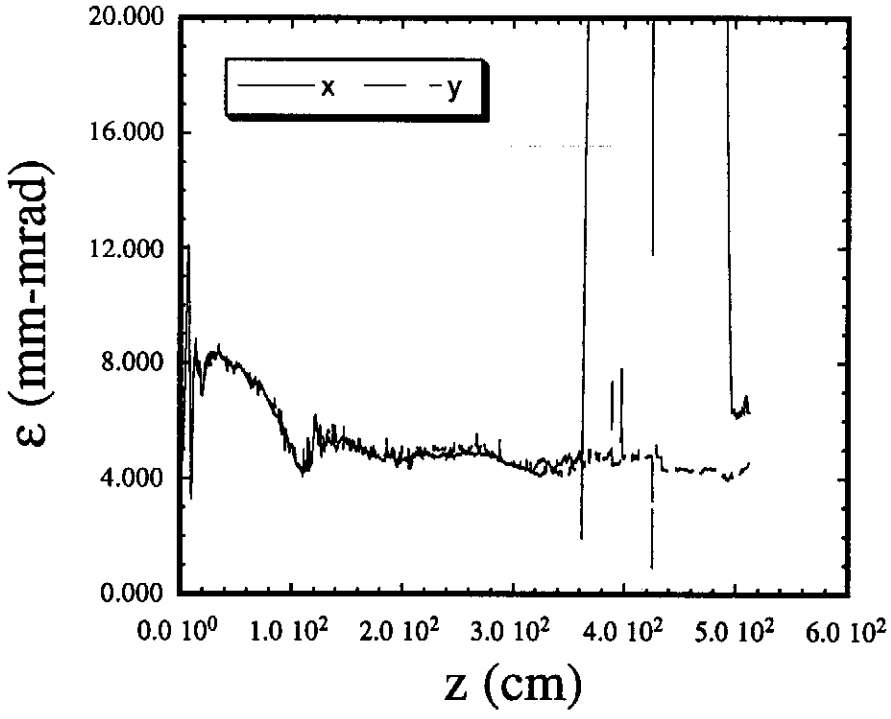

Figure 13. Evolution of rms transverse emittances in rf photoinjector, linac and compressor, 1 nC case.

The final phase space distribution is shown in Figure 14. The rms pulse width associated with this distribution is 0.33 mm, which is very close to what is predicted by the scaling arguments. The final longitudinal emittance, after compression and collimation, is 53 mm-keV, again in good agreement with the predictions of charge scaling.

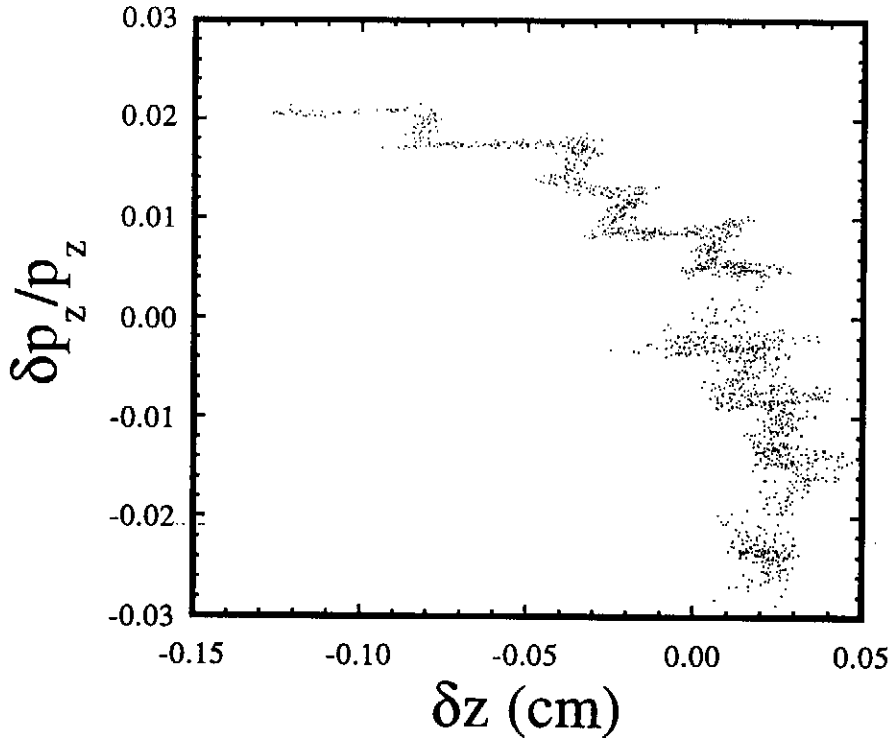

Figure 14. The longitudinal phase space after compression and collimation, 1 nC case.

Note that in the 1 nC longitudinal phase space, the curvature of the distribution due to the rf phase extent of the beam is much less noticeable, and that the current tail has been mitigated. This shows the desirability of using shorter pulses before compression, which allows one to take advantage of a more linear phase space distribution.

VI. Conclusions

The performance of this compressor, while adequate for TTF in this first analysis, could certainly use further work in optimization, and exploration of the parameter space. In particular, one should note that while the this compressor is slightly overdesigned for compressing the 4 mm rms beam to less than one mm rms without collimation, once the tails are removed, the compressor can exceed the nominal compression design goal by a factor of nearly two. Less extreme compression should mitigate the transverse and longitudinal emittance blowup described above. It does not seem necessary to explore qualitatively different designs in order to meet the goals of the TTF injector, but this is not the case for the low charge, high brightness beam for the FEL, as the emittance required is much smaller. Further questions remain about the effects of retardation of the

fields on the emittance performance in particular. This subject, in addition to others, will be investigated by the UCLA group, B. Carlsten of Los Alamos, and the Milan group.

A most promising line of inquiry is being presently pursued by Eric Colby, who has changed the input conditions for the compressor somewhat radically, by shortening the injected laser pulse (while maintaining constant emitted beam density by making the beam radially larger, as is required by charge scaling[4]) in order to linearize the longitudinal phase space distribution, and reduce the longitudinal emittance. The beam does not have to be compressed as much in this case, which means the linac does not have to be run as far off crest. This linearization of the phase space mitigates the problem of generating a relatively long spatial tail in the beam after the compressor. Running closer to the linac crest with a shorter initial beam has the additional effect of lowering the transverse emittance growth, since the energy spread, and the associated coupling to the betatron phase space, is mitigated. The effect of the energy spread on the horizontal emittance can be estimated as follows, by assigning all of the emittance growth to the spread in dispersion mismatch over the beam population;

$$\Delta\varepsilon_x^2 \cong \left\langle \left(\delta\eta_x \frac{\delta p}{p} \right)^2 \right\rangle \left\langle \left(\delta\eta_x' \frac{\delta p}{p} \right)^2 \right\rangle - \left\langle \delta\eta_x \delta\eta_x' \left(\frac{\delta p}{p} \right)^2 \right\rangle^2 \approx \sigma_{\delta p/p}^4 \left[\left\langle \delta\eta_x{}^2 \right\rangle \left\langle \delta\eta_x'^2 \right\rangle - \left\langle \delta\eta_x \delta\eta_x' \right\rangle^2 \right],$$

where $\delta\eta_x \equiv \eta_x - \langle \eta_x \rangle$, and $\delta\eta_x' \equiv \eta_x' - \langle \eta_x' \rangle$.

The term within the square brackets is dependent mostly on the peak current at the end of compression, and so one expects that the emittance growth (added in quadrature) scales approximately as the square of the energy spread. This scaling explains the motivation to begin in the rf gun with a shorter pulse length. Unfortunately, this pulse length is not preserved in the long drift length between the gun and the linac, and thus the energy spread cannot be made arbitrarily small.

As a final example of the performance of the entire rf photoinjector, compressor and transport system (using a laser beam four times shorter than in the initial design), we display in Figures 15 and 16 the behavior of the beam envelopes and emittances from the cathode all the way through the first two cavities of the TTF, using a tentativley adopted layout which has minimal changes to the Injector I setup (the superconducting "capture" cavity, and the analyzing spectrometer are not moved; some quadrupole postions are changed). This is a first attempt at the full analysis of the beam transport, but it shows some promising properties, not the least of which is good matching into the rf focusing[7] of the TTF. It does, on the other hand, have problems associated with emittance growth

due to space charge in the 4.7 m drift between the final quadrupole triplet and the first TTF linac cavity. This and other optimization issues are currently being addressed by continued simulation[6].

While further computational study is necessary, the issues raised here can be most credibly addressed experimentally. Plans are now being formulated to install a chicane at the Phase I experimental test of the TTF photoinjector at ANL.

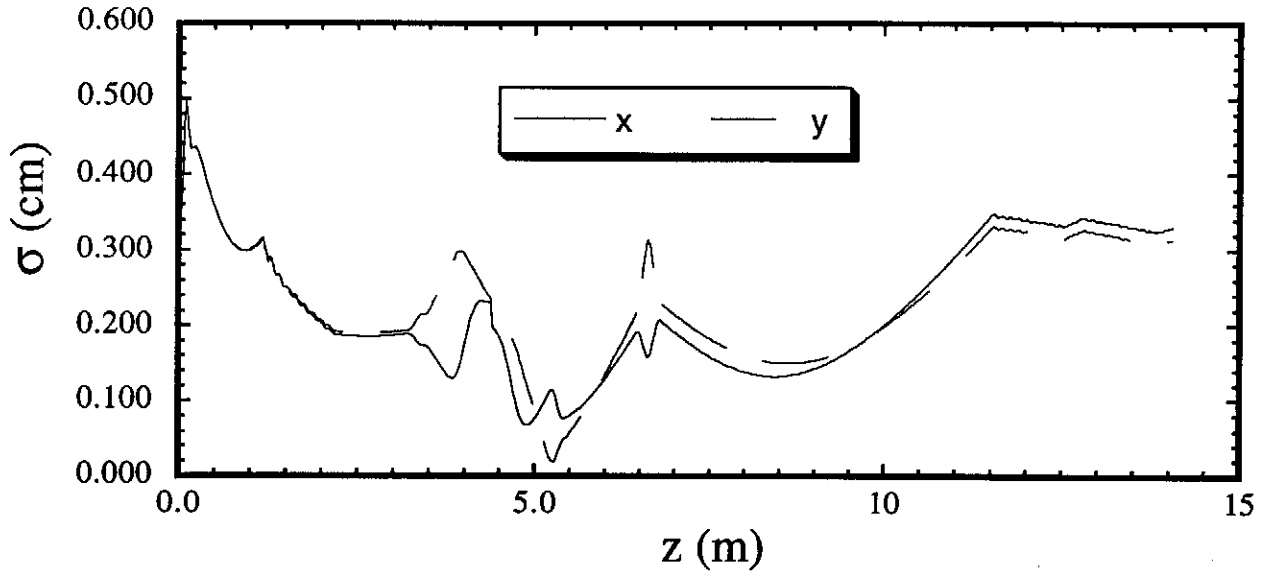

Figure 15: Rms beam sizes through photoinjector, compressor, beam transport and first two TTF linac modules.

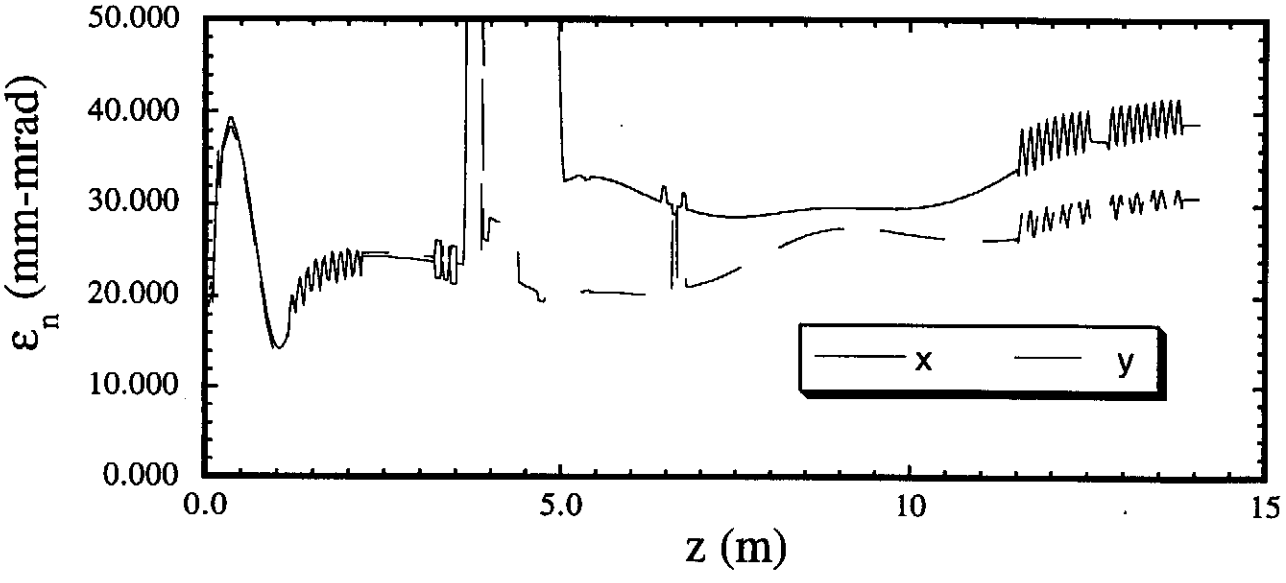

Figure 16: Rms emittances through photoinjector, compressor, beam transport and first two TTF linac modules.

The author thanks B. Carlsten and R. Miller for useful discussions and Eric Colby for his unfailing support in keeping PARMELA alive. This work performed with partial support from U.S. Dept. of Energy grants DE-FG03-90ER40796 and DE-FG03-92ER40693, and the Alfred P. Sloan Foundation grant BR-3225.

REFERENCES

1. B.E. Carlsten, B.D. McVey, E.M. Svaton, and L.M. Young, "Magnetic bunchers for generation of high peak current, low emittance electron pulses at medium energy", *Proc. 1990 Linear Accel. Conf.*, Los Alamos National Laboratory Publication LA-12004-C, Albuquerque NM (1991).

2. K.R. Crandall and D.P. Rusthoi , "TRACE 3D Documentation," Los Alamos National Laboratory Publication LA-11054-MS (1987).

3. E. Colby, J.-F. Ostiguy, and J.B. Rosenzweig, "High brightness, symmetric emittance rf photoinjector preliminary design report", Fermilab TM-1900, September 1994.

4. "Charge and wavelength scaling of rf photoinjector designs", J.B. Rosenzweig and E. Colby, to be published in the *Proceedings of the 1994 Advanced Accelerator Concepts Workshop* (Lake Geneva, 1994).

5. J. Rossbach, presented at TTF injector meeting, October 6, 1994.

6. E. Colby, "Optimization of TTF Injector II Performance", in preparation.

7. J.B. Rosenzweig and L. Serafini, "Transverse Particle Motion In Radio-Frequency Linear Accelerators", *Physical Review E* **49**, 1499 (1994).